

A global (volume averaged) model of a Cl₂/Ar discharge: I. Continuous power

To cite this article: E G Thorsteinsson and J T Gudmundsson 2010 *J. Phys. D: Appl. Phys.* **43** 115201

View the [article online](#) for updates and enhancements.

Related content

- [The low pressure Cl₂/O₂ discharge and the role of ClO](#)
E G Thorsteinsson and J T Gudmundsson
- [A global \(volume averaged\) model of a chlorine discharge](#)
E G Thorsteinsson and J T Gudmundsson
- [A global \(volume averaged\) model of a Cl₂/Ar discharge: II. Pulsed power modulation](#)
E G Thorsteinsson and J T Gudmundsson

Recent citations

- [A global model study of the population dynamics of molecular hydrogen and the generation of negative hydrogen ions in low-pressure ICP discharge with an expansion region: effects of EEPF](#)
Wei Yang *et al*
- [F-atom kinetics in SF₆/Ar inductively coupled plasmas](#)
Wei Yang *et al*
- [A hybrid model of radio frequency biased inductively coupled plasma discharges: description of model and experimental validation in argon](#)
De-Qi Wen *et al*



IOP | **ebooks**TM

Bringing you innovative digital publishing with leading voices to create your essential collection of books in STEM research.

Start exploring the collection - download the first chapter of every title for free.

A global (volume averaged) model of a Cl₂/Ar discharge: I. Continuous power

E G Thorsteinsson¹ and J T Gudmundsson^{1,2,3}

¹ Science Institute, University of Iceland, Dunhaga 3, IS-107 Reykjavik, Iceland

² Department of Electrical and Computer Engineering, University of Iceland, Hjardarhaga 2-6, IS-107 Reykjavik, Iceland

E-mail: tumi@hi.is

Received 16 November 2009, in final form 17 January 2010

Published 4 March 2010

Online at stacks.iop.org/JPhysD/43/115201

Abstract

A global (volume averaged) model is applied to a low pressure (1–100 mTorr) high density chlorine discharge diluted with argon. The model is found to be in fair agreement with measurements reported in the literature. Atomic chlorine is the dominating chlorine species at low pressures and low argon content, but with increasing pressure the discharge becomes less dissociated. As the argon content is increased the chlorine dissociation fraction increases and the decrease with pressure becomes less pronounced. The electronegativity was found to decrease proportionally to the argon dilution for a wide range of discharge conditions. The pressure dependence of the Cl⁺/n₊ fraction was found to vary with argon content, from peaking at low pressures in a pure chlorine discharge to peaking at high pressures in an argon dominated discharge. The electron temperature increases with argon content at low and intermediate pressures but decreases at high pressures. Argon–chlorine reactions generally have only a small effect on the creation or destruction of chlorine particles, even at high argon content, except for the loss of Cl[−] which is rapidly neutralized by Ar⁺ ions in an argon dominated discharge. Surface losses are most important for positive ion loss at low pressures and become increasingly important when the chamber is made larger or argon is added to the discharge. Volume losses always dominate the loss of neutral Cl atoms at low pressures, but at moderate to high pressures as well when the chamber is either large or small. Argon dilution benefits the neutral surface losses in small chambers but the volume losses in large chambers.

(Some figures in this article are in colour only in the electronic version)

1. Introduction

The chlorine molecule has a low dissociation energy (2.5 eV) and a near-zero threshold energy for dissociative attachment which is almost the sole contributor to the creation of the negative ion Cl[−] in a chlorine discharge [1]. The chlorine discharge is highly dissociated and highly electronegative in the pressure range 1–100 mTorr. Chlorine and its mixtures are widely used for thin film etching, in particular poly-silicon. The etching of various thin films has been demonstrated in Cl₂/Ar chemistry, including SiO₂ and MgO [2], Ta and TaN [3], ZnO [4], ZrO₂ [5] and Bi_{4-x}La_xTi₃O₁₂ [6]. Shin *et al* [3] suggest that Cl radical density plays an important role in determining the etch rate and that the radical density is considerably influenced by the Cl₂/Ar mixing ratio. Gu *et al* [2]

report a maximum in the etch rate for a 70% Cl₂/30% Ar mixing ratio when etching SiO₂ and a maximum in the etch rate for a 30% Cl₂/70% Ar mixing ratio when etching MgO at 10 mTorr. The etching characteristics of Cl₂/Ar discharges have also been studied theoretically. Efremov *et al* [7, 8] and Kleditzsch and Riedel [9] developed volume averaged models to explore the influence of Cl₂/Ar mixing ratio on the etch rate of silicon in Cl₂/Ar plasmas. Tinck *et al* [10] studied the effect of bias, power and pressure on the etch rate in an Ar/Cl₂ discharge with a hybrid plasma model. Their calculations suggested that the etch rate is more strongly affected by the energy and flux of the ions bombarding the substrate than by the magnitude of the radical flux. The plasma parameters in Cl₂/Ar discharges have been studied by several authors. Corr *et al* [11] compared fluid simulations with measurements of electronegativity and electron density

³ Author to whom any correspondence should be addressed.

in an Ar/Cl₂ discharge and found that the calculated charged particle densities were systematically overestimated by a factor of 3–5. However, the agreement between the calculated and measured electronegativity was good. Fuller *et al* [12, 13] measured the electron temperature and particle densities in an inductively coupled Cl₂/Ar discharge and found that the ratio of neutral to charged particle flux was strongly dependent on the argon dilution. Bassett and Economou [14] investigated the effect of Cl₂ addition to an argon glow discharge with a global model and found a dramatic difference between a pure argon and a 5% Cl₂/95% Ar discharge. Eddy *et al* [15] performed an extensive experimental characterization of the Cl₂/Ar discharge versus power, pressure and the argon/chlorine mixing ratio. The spatially resolved electron density, electron temperature and plasma potential were found with three-dimensional Langmuir probe measurements and the relative volume averaged particle densities with optical emission and mass spectrometric measurements. They reported that chlorine dilution to an argon plasma mostly affected the neutral particle densities, having an insignificant effect on the electron density or charged particle fluxes.

In this study, which is part I in a series of two papers, we present and apply a global (volume averaged) model to investigate the influence of argon dilution on the chlorine dissociation fraction, the electronegativity, the fraction of Cl⁺ positive ions and the reaction mechanisms in a Cl₂/Ar discharge when the applied power is continuous. In part II [16] we will explore the plasma parameters of the Cl₂/Ar discharge when the applied power is pulse modulated.

2. The global (volume averaged) model

We assume a cylindrical chamber of radius R and length L . A steady flow Q of neutral species (Cl₂ and Ar) is introduced through the inlet. The content of the chamber is assumed to be nearly spatially uniform and the power is deposited uniformly into the plasma bulk. The outlet-flow pressure, which partially controls the pumping of gas out of the chamber, is adjusted to establish the correct discharge pressure p , which is defined as the sum of all partial pressures in the discharge. Electrons are assumed to have a Maxwellian-like energy distribution function and the electron collision rate coefficients are calculated and fitted to analytical forms over the electron temperature range $0.01 < T_e < 10$ V. In addition to electrons, the discharge consists of ground state chlorine molecules Cl₂($X^1\Sigma_g^+$, $v = 0$), vibrationally excited chlorine molecules Cl₂($X^1\Sigma_g^+$, $v = 1\text{--}3$) ($\mathcal{E}_{\text{ex}} = 0.07\text{--}0.21$ eV), ground state chlorine atoms Cl(3p²P), negative chlorine ions Cl⁻ ($\mathcal{E}_{\text{aff}} = 3.6$ eV), positive chlorine ions Cl⁺ ($\mathcal{E}_{\text{iz}} = 13.0$ eV) and Cl₂⁺ ($\mathcal{E}_{\text{iz}} = 11.5$ eV), ground state argon Ar(3s²3p⁶), metastable argon Ar^m (1s₅ and 1s₃) ($\mathcal{E}_{\text{ex}} = 11.6$ eV), radiatively coupled levels Ar^r (1s₄ and 1s₂) ($\mathcal{E}_{\text{ex}} = 11.7$ eV), higher excited argon Ar(4p) ($\mathcal{E}_{\text{ex}} = 13.2$ eV) and positive argon ions Ar⁺ ($\mathcal{E}_{\text{iz}} = 15.8$ eV).

The plasma chemistry is described by a set of non-linear equations $\mathbf{F}(y, t) = \mathbf{0}$; a particle balance equation for each of the species included in the discharge and one power balance equation describing the conservation of energy

[17, 18], 14 equations in total. This system of equations is solved simultaneously by iteration with the MATLAB function fsolve, giving the particle densities and electron temperature.

2.1. Particle balance

The particle balance equation for a species X is given by

$$\frac{dn^{(X)}}{dt} = \sum_i R_{\text{Generation},i}^{(X)} - \sum_i R_{\text{Loss},i}^{(X)}, \quad (1)$$

where $R_{\text{Generation},i}^{(X)}$ and $R_{\text{Loss},i}^{(X)}$, respectively, are the reaction rates of the various generation and loss processes of species X . In this study we consider a variety of processes for the loss and generation of the discharge species, including reactions between electrons and gas species and between two (or more) gas species in the bulk plasma, recombination and quenching of neutral species and neutralization of positive ions on the chamber walls, as well as pumping of gas species into (Cl₂ and Ar) and out of the chamber (all neutrals and positive ions). The reaction rate R for a given reaction is calculated as the product of the reactants' densities and the rate coefficient k of the reaction:

$$R = k \times \prod_i n_{r,i} (\text{m}^{-3} \text{s}^{-1}), \quad (2)$$

where $n_{r,i}$ is the density of the i th reactant. Since the discharge is assumed to be quasi-neutral,

$$n_e = [\text{Ar}^+] + [\text{Cl}^+] + [\text{Cl}_2^+] - [\text{Cl}^-], \quad (3)$$

where $[X]$ is the density of species X , an equation describing the particle balance of free electrons is not required.

The reaction set is summarized in table 1. A more elaborate discussion on the chlorine reaction set is given elsewhere [1, 19]. Although the choice of cross-sections or rate coefficients has not changed, we have improved the low energy portions of some of the cross-sections by adding zeros at their threshold or appearance energies. Having been given only from 8.4 eV previously, a zero value at 4 eV was added to the cross-section for electron impact dissociation, reaction (R1), in accordance with the cross-section calculated by Rescigno [20]. A zero value was also added to the cross-section for polar dissociation, reaction (R6), at 11.9 eV, which is the threshold energy of the reaction. Although just a minor modification, the cross-section for ionization of Cl, reaction (R13), was changed to be absolute zero below the ionization threshold, 13 eV, instead of the previous near-zero values. The argon reaction set is an updated version of the reaction set used for a previous study of a continuous power O₂/Ar discharge [21]. With the exception of reactions (R29) and (R30), the data for most of the electron impact reactions were revised, primarily because cross-section data are now preferred over rate coefficient data. The rate coefficients for the various argon–argon collisions were on the other hand retained. The rate coefficient for ion–ion recombination of Cl⁻ and Ar⁺, reaction (R41), was modified in the same manner as for the corresponding reactions with Cl₂⁺ and Cl⁺, reactions (R16) and (R17), adding the

Table 1. The reaction set for the Cl_2/Ar discharge. The rate coefficients for electron impact collisions are calculated assuming a Maxwellian-like electron energy distribution function and fitted in the range $T_e = 0.01\text{--}10\text{ V}$.

Reaction	Rate coefficient ($\text{m}^3 \text{s}^{-1}$)	References	Note
(R1) $e + \text{Cl}_2(v=0) \rightarrow \text{Cl} + \text{Cl} + e$	$1.04 \times 10^{-13} T_e^{-0.29} e^{-8.84/T_e}$	[28]	a
(R2) $e + \text{Cl}_2(v=0) \rightarrow \text{Cl}_2^+ + 2e$	$5.12 \times 10^{-14} T_e^{0.48} e^{-12.34/T_e}$	[29]	a
(R3) $e + \text{Cl}_2(v=0) \rightarrow \text{Cl} + \text{Cl}^+ + 2e$	$2.14 \times 10^{-13} T_e^{-0.07} e^{-25.26/T_e}$	[29, 30]	a
(R4) $e + \text{Cl}_2(v=0) \rightarrow \text{Cl}^+ + \text{Cl}^+ + 3e$	$2.27 \times 10^{-16} T_e^{1.92} e^{-21.26/T_e}$	[29, 30]	a
(R5) $e + \text{Cl}_2(v=0) \rightarrow \text{Cl} + \text{Cl}^-$	$3.43 \times 10^{-15} T_e^{-1.18} e^{-3.98/T_e} + 3.05 \times 10^{-16} T_e^{-1.33} e^{-0.11/(T_e+0.014)}$	[23, 31, 32]	b
(R6) $e + \text{Cl}_2(v=0) \rightarrow \text{Cl}^+ + \text{Cl}^- + e$	$2.94 \times 10^{-16} T_e^{0.19} e^{-18.79/T_e}$	[31, 33]	a
(R7) $e + \text{Cl}_2(v=0) \rightarrow \text{Cl}_2(v=1) + e$	$1.22 \times 10^{-16} T_e^{-0.99} e^{-0.40/T_e} + 1.88 \times 10^{-16} e^{-(\ln(T_e)+1.01)^2/(2\times 1.10^2)}$	[34]	c
(R8) $e + \text{Cl}_2(v=0) \rightarrow \text{Cl}_2(v=2) + e$	$3.28 \times 10^{-17} T_e^{-1.12} e^{-0.37/T_e} + 2.86 \times 10^{-17} e^{-(\ln(T_e)+0.99)^2/(2\times 1.06^2)}$	[34]	c
(R9) $e + \text{Cl}_2(v=0) \rightarrow \text{Cl}_2(v=3) + e$	$1.30 \times 10^{-17} T_e^{-1.24} e^{-0.41/T_e} + 6.08 \times 10^{-18} e^{-(\ln(T_e)+0.94)^2/(2\times 1.02^2)}$	[34]	c
(R10) $e + \text{Cl}_2(v=1) \rightarrow \text{Cl}_2(v=2) + e$	$3.00 \times 10^{-16} T_e^{-1.00} e^{-0.37/T_e} + 4.61 \times 10^{-16} e^{-(\ln(T_e)+1.04)^2/(2\times 1.10^2)}$	[34]	c, d
(R11) $e + \text{Cl}_2(v=1) \rightarrow \text{Cl}_2(v=3) + e$	$1.25 \times 10^{-16} T_e^{-1.13} e^{-0.36/T_e} + 1.06 \times 10^{-16} e^{-(\ln(T_e)+1.01)^2/(2\times 1.06^2)}$	[34]	c
(R12) $e + \text{Cl}_2^+ \rightarrow \text{Cl} + \text{Cl}$	$9.00 \times 10^{-14} T_e^{-0.50}$	[1, 19]	e
(R13) $e + \text{Cl} \rightarrow \text{Cl}^+ + e + e$	$3.17 \times 10^{-14} T_e^{0.53} e^{-13.29/T_e}$	[35, 36]	
(R14) $e + \text{Cl}^- \rightarrow \text{Cl} + e + e$	$9.02 \times 10^{-15} T_e^{0.92} e^{-4.88/T_e}$	[37]	
(R15) $e + \text{Cl}^- \rightarrow \text{Cl}^+ + 3e$	$3.62 \times 10^{-15} T_e^{0.72} e^{-25.38/T_e}$	[37]	
(R16) $\text{Cl}_2^+ + \text{Cl}^- \rightarrow 3\text{Cl}$	$5.00 \times 10^{-14} (300/T_g)^{0.50}$	[22, 38]	
(R17) $\text{Cl}^+ + \text{Cl}^- \rightarrow \text{Cl} + \text{Cl}$	$5.00 \times 10^{-14} (300/T_g)^{0.50}$	[22, 38, 39]	
(R18) $\text{Cl}_2 + \text{Cl}^+ \rightarrow \text{Cl} + \text{Cl}_2^+$	5.40×10^{-16}	[40]	f
(R19) $2\text{Cl} + \text{Cl}_2 \rightarrow \text{Cl}_2 + \text{Cl}_2$	$3.50 \times 10^{-45} e^{810/T_g} \text{ m}^6 \text{ s}^{-1}$	[41]	f
(R20) $2\text{Cl} + \text{Cl} \rightarrow \text{Cl}_2 + \text{Cl}$	$8.75 \times 10^{-46} e^{810/T_g} \text{ m}^6 \text{ s}^{-1}$	[41, 42]	
(R21) $e + \text{Ar} \rightarrow \text{Ar}^+ + e + e$	$2.39 \times 10^{-14} T_e^{0.57} e^{-17.43/T_e}$	[43]	
(R22) $e + \text{Ar}^m \rightarrow \text{Ar}^+ + e + e$	$2.71 \times 10^{-13} T_e^{0.26} e^{-4.59/T_e}$	[44]	
(R23) $e + \text{Ar}^r \rightarrow \text{Ar}^+ + e + e$	$2.70 \times 10^{-13} T_e^{0.29} e^{-4.24/T_e}$	[44]	
(R24) $e + \text{Ar} \rightarrow \text{Ar}^m + e$	$9.73 \times 10^{-16} T_e^{-0.07} e^{-11.69/T_e}$	[45]	c
(R25) $e + \text{Ar} \rightarrow \text{Ar}^r + e$	$3.93 \times 10^{-15} T_e^{0.46} e^{-12.09/T_e}$	[46]	c
(R26) $e + \text{Ar} \rightarrow \text{Ar}(4p) + e$	$8.91 \times 10^{-15} T_e^{-0.04} e^{-14.18/T_e}$	[46]	c
(R27) $e + \text{Ar}(4p) \rightarrow \text{Ar}^+ + e + e$	$1.09 \times 10^{-12} T_e^{0.29} e^{-3.42/T_e}$	[47]	
(R28) $e + \text{Ar}^m \rightarrow \text{Ar}(4p) + e$	$2.39 \times 10^{-12} T_e^{-0.15} e^{-1.82/T_e}$	[45]	c, g
(R29) $e + \text{Ar}^m \rightarrow \text{Ar}^r + e$	3.70×10^{-13}	[21]	
(R30) $e + \text{Ar}^r \rightarrow \text{Ar}^m + e$	9.10×10^{-13}	[21]	
(R31) $\text{Ar}^m + \text{Ar}^m \rightarrow \text{Ar} + \text{Ar}$	2.00×10^{-13}	[21]	
(R32) $\text{Ar}^m + \text{Ar}^r \rightarrow \text{Ar} + \text{Ar}^+ + e$	2.10×10^{-15}	[21]	
(R33) $\text{Ar}(4p) + \text{Ar}(4p) \rightarrow \text{Ar} + \text{Ar}^+ + e$	5.00×10^{-16}	[21]	
(R34) $\text{Ar}^m + \text{Ar}^m \rightarrow \text{Ar} + \text{Ar}^+ + e$	6.40×10^{-16}	[21]	
(R35) $\text{Ar} + \text{Ar}^m \rightarrow \text{Ar} + \text{Ar}$	2.10×10^{-21}	[21]	
(R36) $\text{Ar}^r \rightarrow \text{Ar} + \hbar\omega$	$1.00 \times 10^5 \text{ s}^{-1}$	[21]	
(R37) $\text{Ar}(4p) \rightarrow \text{Ar} + \hbar\omega$	$3.20 \times 10^7 \text{ s}^{-1}$	[21]	
(R38) $\text{Ar}(4p) \rightarrow \{\text{Ar}^m, \text{Ar}^r\} + \hbar\omega$	$3.00 \times 10^7 \text{ s}^{-1}$	[21]	
(R39) $\text{Cl}_2 + \text{Ar}^+ \rightarrow \text{Cl}_2^+ + \text{Ar}$	1.90×10^{-16}	[24]	
(R40) $\text{Cl}_2 + \text{Ar}^+ \rightarrow \text{Cl} + \text{Cl}^+ + \text{Ar}$	5.70×10^{-16}	[24]	
(R41) $\text{Cl}^- + \text{Ar}^+ \rightarrow \text{Cl} + \text{Ar}$	$5.00 \times 10^{-14} (300/T_g)^{0.50}$	[14, 22]	
(R42) $\text{Cl}_2 + \text{Ar}^* \rightarrow \text{Cl}_2^+ + \text{Ar} + e$	7.10×10^{-16}	[48]	h
(R43) $\text{Cl} + \text{Ar}^+ \rightarrow \text{Cl}^+ + \text{Ar}$	2.00×10^{-16}	[48]	
(R44) $2\text{Cl} + \{\text{Ar}, \text{Ar}^*\} \rightarrow \text{Cl}_2 + \text{Ar}$	$8.75 \times 10^{-46} e^{-810/T_g} \text{ m}^6 \text{ s}^{-1}$	[41, 42]	h
T_e (V)			
T_g (K)			

^a The cross-sections for $\text{Cl}_2(v > 0)$ reactants are obtained by reducing the threshold of the original cross-section by $v \times 0.07\text{ eV}$.

^b The cross-sections for $\text{Cl}_2(v=1\text{--}3)$ reactants are obtained by multiplying this cross-section by 4.1, 8.8 and 13.5, respectively [1, 32].

^c The cross-section for the corresponding de-excitation is obtained by applying the principle of detailed balancing [22, 25].

^d The cross-section for the transition $v = 2 \rightarrow 3$ is assumed to be identical to this cross-section.

^e Estimated from dissociative recombination rate coefficients for other elements (see references).

^f Cl_2 stands for $\text{Cl}_2(v=0\text{--}3)$, i.e. any of the neutral chlorine molecules included in the model.

^g The cross-section for an Ar^r reactant is obtained by reducing the threshold of this cross-section by 0.09 eV.

^h Ar^* stands for $\{\text{Ar}^m, \text{Ar}^r, \text{Ar}(4p)\}$, i.e. any of the excited argon atoms included in the model.

term $(300/T_g)^{1/2}$ according to the analysis of Liebermann and Lichtenberg [22, p 258]. Since charge transfer from Ar^+ to Cl_2 ,



is exothermic by 4.3 eV and the dissociation energy of Cl_2^+ is roughly 4 eV [23], the resulting Cl_2^+ ion has a high probability of dissociating. In addition to measuring the rate coefficient at 300 K, Španěl *et al* [24] reported a branching ratio of 0.25 : 0.75

for non-dissociative and dissociative charge transfer, reactions (R39) and (R40), respectively. The rate coefficients for electron impact reactions are found by averaging the corresponding electron energy dependent cross-section, $\sigma(\mathcal{E})$, over the assumed electron energy distribution function $f(\mathcal{E})$ [25]:

$$k(T_e) = \left(\frac{2e}{m_e} \right)^{1/2} \int_0^\infty \sigma(\mathcal{E}) \mathcal{E}^{1/2} f(\mathcal{E}) d\mathcal{E}. \quad (4)$$

In the previous studies [1, 21] the electron collision rate coefficients were calculated and fitted to the modified Arrhenius form over the electron temperature range $1 < T_e < 7$ V. However, here the rate coefficients presented in table 1 were fitted over the electron temperature range $0.01 < T_e < 10$ V since the electron temperature in pulsed discharges, which is studied in the second part of this paper [16], is known to spike when the power is turned on and approach zero some time after the power has been turned off. This will alter the expressions for some, if not all, of the rate coefficients. Although the vast majority of the rate coefficients are zero below $T_e = 1$ V, the rate coefficients for processes such as dissociative electron attachment and vibrational excitation are larger at low electron temperatures. We were unable to find an acceptable fit for these rate coefficients to the modified Arrhenius form, as normally used for electron collision rate coefficients. We found that we could fit the rate coefficient for dissociative electron attachment accurately over the entire range of electron temperatures by adding a term of the form

$$A \times T_e^B \times \exp(-C/(T_e + D)) \quad (5)$$

to the modified Arrhenius form. For the vibrational excitation rate coefficients, we found that a more suitable equation was the sum of the modified Arrhenius equation and a Gaussian function:

$$a \times \exp(-(ln(T_e) - b)^2/2c^2). \quad (6)$$

These functions provide a basis for accurate fits to the rate coefficients while being considerably less complex and more similar to the modified Arrhenius equation than the rate coefficients presented elsewhere [26, 27].

2.2. Power balance

The power balance equation, which equates the absorbed power to power losses due to elastic and inelastic collisions and losses due to charged particle flow to the walls, is given as [49]

$$\left[\frac{P_{\text{abs}}(t)}{V} - e n_e \sum_X n^{(X)} \mathcal{E}_c^{(X)} k_{iz}^{(X)} - e u_{B0} n_i \frac{A_{\text{eff}}}{V} (\mathcal{E}_i + \mathcal{E}_e) \right] = \frac{d}{dt} \left(\frac{3}{2} e n_e T_e \right) = \frac{d}{dt} \left(\frac{3}{2} p_e \right), \quad (7)$$

where $P_{\text{abs}}(t)$ is the absorbed power, which is constant in the current continuous power study and from this point onwards denoted as simply P_{abs} , p_e is the thermal electron energy density, $u_{B0} = (e T_e / m_i)^{1/2}$ is the Bohm velocity of positive ions with mass m_i , V is the volume of the discharge chamber, $A_{\text{eff}} = 2\pi(R^2 h_L + RL h_R)$ is the effective surface area for ion

Table 2. The threshold energies and the references to the cross-sections used for collisions of electrons with argon atoms leading to a collisional electron energy loss.

Final state	Thresh. (eV) [51, 52]	Cross section
4s[3/2]₂	11.6	[46]
4s[3/2]₁	11.6	[46]
4s'[1/2]₀	11.7	[46]
4s'[1/2]₁	11.8	[46]
4p[1/2]₁	12.9	[46]
4p[5/2]₃	13.1	[46]
4p[5/2]₂	13.1	[46]
4p[3/2]₁	13.2	[46]
4p[3/2]₂	13.2	[46]
4p[1/2]₀, 4p'[3/2]₁	13.3	[46]
4p'[3/2]₂	13	[46]
4p'[1/2]₁	13.3	[46]
4p'[1/2]₀	13.5	[46]
3d[1/2]₀, 3d[1/2]₁	13.8	[46]
3d[3/2]₂	13.9	[46]
3d[7/2]₄	14	[46]
3d[7/2]₃	14	[46]
3d[5/2]₂, 5s[3/2]₂	14.1	[46]
3d[5/2]₃, 5s[3/2]₁	14.1	[46]
3d[3/2]₁	14.2	[46]
3d'[5/2]₂	14.2	[46]
3d'[5/2]₃, 3d'[3/2]₂,		
5s'[1/2]₀, 5s'[1/2]₁	14.2	[46]
3d'[3/2]₁	14.3	[46]
4d[1/2]₁	14.7	[46]
6p'[1/2]₁, 6p'[3/2]₁,		
6p'[3/2]₂	15.2	[46]
Ionization	15.8	[43]
Elastic scattering	$3m_e/m_{Ar} T_e$	[46]

loss, h_L and h_R are the axial and radial edge to centre positive ion density ratios given in section 2.4, n_e is the electron density, n_i is the positive ion density and $\mathcal{E}_e = 2T_e$ is the mean kinetic energy per electron lost. The mean kinetic energy per ion lost \mathcal{E}_i is modified by the electronegativity as discussed elsewhere [1]. The sum is over all ground state neutral particles X (Cl_1 , Cl_2 and Ar), having density $n^{(X)}$, ionization rate coefficient $k_{iz}^{(X)}$ and collisional energy loss per electron-ion pair created $\mathcal{E}_c^{(X)}$, given as [50]

$$\mathcal{E}_c^{(X)} = \mathcal{E}_{iz}^{(X)} + \sum_i \mathcal{E}_{ex,i}^{(X)} \frac{k_{ex,i}^{(X)}}{k_{iz}^{(X)}} + \frac{k_{el}^{(X)}}{k_{iz}^{(X)}} \frac{3m_e}{m^{(X)}} T_e, \quad (8)$$

where $\mathcal{E}_{iz}^{(X)}$ is the ionization energy of species X , $\mathcal{E}_{ex,i}^{(X)}$ and $k_{ex,i}^{(X)}$ are the excitation energy and rate coefficient for the i th excitation process of species X , respectively, $k_{el}^{(X)}$ is the elastic scattering rate coefficient of species X , m_e is the electron mass and $m^{(X)}$ is the mass of species X .

The set of reactions contributing to the collisional energy loss of each electron- Ar^+ pair created, $\mathcal{E}_c^{(\text{Ar})}$, is summarized in table 2. The set of processes that are used in the calculation of $\mathcal{E}_c^{(\text{Cl}_1)}$ and $\mathcal{E}_c^{(\text{Cl}_2)}$ are summarized elsewhere [1]. Similarly to the other rate coefficients, the rate coefficient for the collisional energy loss calculation are fitted over the electron temperature range 0.01–10 V. The rate coefficients for vibrational excitation of Cl_2 and for elastic scattering of Cl and Ar could not be accurately fitted to the modified Arrhenius form. A simple

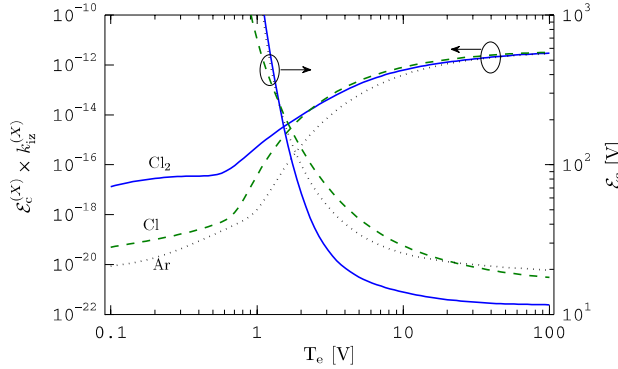


Figure 1. The product of the collisional energy loss for each electron-ion pair created $\mathcal{E}_c^{(X)}$ and the ionization rate coefficient $k_{iz}^{(X)}$ versus the electron temperature T_e for $X = \text{Cl}_2, \text{Cl}$ and Ar . The collisional energy loss \mathcal{E}_c is also shown for reference on the right axis.

Gaussian function, equation (6), was better suited for the elastic scattering rate coefficients.

The collisional energy loss \mathcal{E}_c and the product of the collisional energy loss and the ionization rate coefficient $\mathcal{E}_c k_{iz}$, as used in equation (7) for the power loss due to inelastic and elastic collisions, is shown in figure 1 versus the electron temperature for Cl_2 , Cl and Ar . Although argon has the largest and second largest collisional energy loss \mathcal{E}_c at electron temperatures below and above 1 V, respectively, its ionization rate coefficient ($\mathcal{E}_{iz} = 15.8 \text{ eV}$) is much smaller than for either Cl ($\mathcal{E}_{iz} = 13.0 \text{ eV}$) or Cl_2 ($\mathcal{E}_{iz} = 11.5 \text{ eV}$) at all electron temperatures. As a consequence, power losses due to elastic and inelastic electron–argon collisions are much smaller relative to Cl and Cl_2 . The collisional energy loss for the Cl atom is much higher than for the Cl_2 molecule at electron temperatures above 1 V. The elastic and inelastic collisional power losses due to Cl atoms are therefore similar or slightly larger relative to that of Cl_2 molecules at electron temperatures above 2 V. At electron temperatures below 1 V $\mathcal{E}_c k_{iz}$ for Cl_2 is about 10–300 times larger than for Cl and about 200–1800 times larger than for Ar .

2.3. The gas temperature

Since the gas temperature in an argon discharge [53] does not seem to be radically different from that in a Cl_2 discharge [54], we will assume argon and chlorine particles are isothermal with the same dependence on power P_{abs} and pressure p as we have found for the Cl_2 discharge [1]:

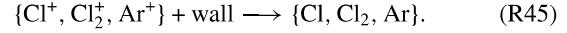
$$T_g(P_{\text{abs}}, p) = 300 + s(p) \times \log_{10}(P_{\text{abs}}/40), \quad (9a)$$

$$s(p) = 780(1 - e^{-0.091 \times p}) + 250 e^{-0.337 \times p}, \quad (9b)$$

which is based on the measurements of Donnelly and Malyshev [54]. Furthermore, we assume that the gas temperature depends only on the average power \bar{P}_{abs} and not the instantaneous power $P_{\text{abs}}(t)$ when the discharge is time modulated. Ion heating, which can be expected in the pulsed mode in particular [55], is neglected as well.

2.4. Surface interactions

Positive ions are lost very effectively as they bombard the chamber walls:



The rate coefficient for the flux of positive ions to the walls is given by

$$k_{+, \text{wall}} = u_{B0} \frac{A_{\text{eff}}}{V} \text{ s}^{-1}, \quad (10)$$

where $u_{B0} = (eT_e/m_i)^{1/2}$ is the Bohm velocity and $A_{\text{eff}} = 2\pi(R^2 h_L + RL h_R)$ is the effective area for ion loss. The axial and radial edge to centre positive ion density ratios h_L and h_R were found for an electronegative discharge in our previous study of the continuous power chlorine discharge [1]. Here, we have modified the expressions to account for diffusion at high pressures, which may be important in weakly electronegative or electropositive discharges, by incorporating the diffusion terms found in earlier expressions of h_L and h_R [25, 27]. Now, the scaling factors are given by the ansatz

$$h_{\{R,L\}} = \left[\left(\frac{h_{\{R,L\},0}}{1 + \alpha_0} \right)^2 + h_c^2 \right]^{1/2}, \quad (11)$$

where $\alpha_0 \approx (3/2)\alpha$ [27] is the central electronegativity, $h_{R,0}$ and $h_{L,0}$ are the zero-electronegativity scaling factors,

$$h_{R,0} = 0.80 \left[4 + \frac{\eta R}{\lambda_i} + \left(\frac{0.80 R u_B}{\chi_{01} J_1(\chi_{01}) D_a} \right)^2 \right]^{-1/2}, \quad (12a)$$

$$h_{L,0} = 0.86 \left[3 + \frac{\eta L}{2\lambda_i} + \left(\frac{0.86 L u_B}{\pi D_a} \right)^2 \right]^{-1/2}, \quad (12b)$$

where $J_1(\chi)$ is the first order Bessel function, $\chi_{01} \simeq 2.405$ is the first zero of the zero order Bessel function J_0 , $\eta = 2T_+/(T_+ + T_-)$, $D_a = D_i(1 + \gamma + \gamma\alpha_s)/(1 + \gamma\alpha_s)$ is the ambipolar diffusion coefficient, D_i is the diffusion coefficient [22] for positive ions, $\gamma = T_e/T_i$ is the fraction of the electron and ion temperatures, $\lambda_i = 1/\sum_j n_j \sigma_{sc,j}$ is the mean free path of ions [22] and α_s is the electronegativity at the sheath edge, whose relation with the bulk electronegativity α is discussed in our previous study of the chlorine discharge [1]. In the mean free path calculations we have assumed that σ_{sc} for Ar and Ar^+ scattering corresponds exactly to σ_{sc} for Cl and Cl^+ scattering, which is also given elsewhere [1]. The mean free path λ is typically in the range 1–2 cm for neutral molecules and atoms and 0.5–1 cm for ions in this study at 10 mTorr. The second term in equation (11) is the scaling factor for a one-region flat-topped electronegative profile [56]:

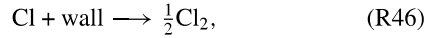
$$h_c \simeq \frac{1}{\gamma_-^{1/2} + \gamma_+^{1/2} [n_*^{1/2} n_+ / n_-^{3/2}]}, \quad (13)$$

where $\gamma_- = T_e/T_-$ and $\gamma_+ = T_e/T_+$ are the electron to negative and positive ion temperature ratios, respectively, and

$$n_* = \frac{15}{56} \frac{\eta^2}{k_{\text{rec}} \lambda_i} v_i, \quad (14)$$

where $v_i = (8kT_i/\pi m_i)^{1/2}$ is the mean thermal velocity of positive ions and $k_{\text{rec}} \simeq 5 \times 10^{-14} (300/T_g)^{1/2} \text{ m}^3 \text{ s}^{-1}$ is the rate coefficient for ion-ion recombination in the bulk plasma. These scaling factors capture the modification to the Bohm velocity due to the presence of negative ions near the sheath edge [56] and are valid for both electronegative (e.g. pure Cl_2) and electropositive (e.g. pure Ar) discharges.

Recombination of neutral atoms on the wall,



is considered to be the single most important reaction for Cl atom loss in the highly dissociated chlorine discharge. The diffusional losses of the neutral chlorine atoms to the reactor walls are estimated by an effective loss-rate coefficient, given by [57]

$$k_{\text{Cl,wall}} = \left[\frac{\Lambda_{\text{Cl}}^2}{D_{\text{Cl}}} + \frac{2V(2 - \gamma_{\text{rec}})}{Av_{\text{Cl}}\gamma_{\text{rec}}} \right]^{-1} \text{ s}^{-1}, \quad (\text{15})$$

where D_{Cl} is the diffusion coefficient for neutral chlorine atoms [22], $v_{\text{Cl}} = (8kT_g/\pi m_{\text{Cl}})^{1/2}$ is the mean Cl velocity, γ_{rec} is the wall recombination coefficient for neutral chlorine atoms on the wall surface, V and A are the volume and the surface area of the reactor chamber, respectively, and Λ_{Cl} is the effective diffusion length of neutral chlorine atoms, given by [58]

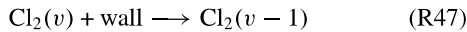
$$\Lambda_{\text{Cl}} = \left[\left(\frac{\pi}{L} \right)^2 + \left(\frac{2.405}{R} \right)^2 \right]^{-1/2}. \quad (\text{16})$$

The wall recombination coefficient γ_{rec} is one of the most important parameters in chlorine discharge modelling. Stafford *et al* [59] measured the wall recombination coefficient of chlorine atoms in a stainless steel chamber and found a relationship between its value and the extent of dissociation in the discharge. We have previously found a fit to γ_{rec} as a function of $[\text{Cl}]/[\text{Cl}_2]$ based on these data:

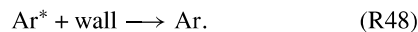
$$\log_{10}(\gamma_{\text{rec}}) = -1.22 - 1.34 \exp \left(-1.48 \times \frac{[\text{Cl}]}{[\text{Cl}_2]} \right), \quad (\text{17})$$

which was found to reproduce excellent agreement with atomic density measurements [1]. Therefore, we have retained this expression for the wall recombination coefficient in this study.

The vibrationally excited chlorine molecules $\text{Cl}_2(v > 0)$ and the excited argon atoms Ar^m , Ar^r and $\text{Ar}(4p)$ are all assumed to be quenched at the chamber surface, i.e.



and



We assume that the rate coefficient for wall quenching is analogous to that for the diffusional losses of neutral atoms at the wall, given by equation (15). The wall quenching probability γ_Q , as used in equation (15) instead of γ_{rec} , is assumed to be unity for quenching of both $\text{Cl}_2(v)$ and Ar^* at the wall.

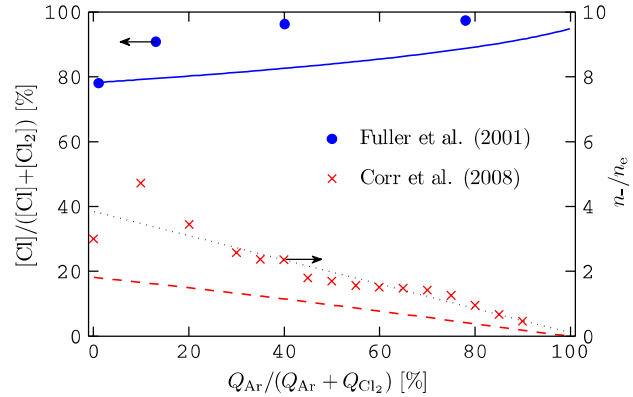
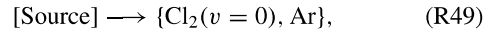


Figure 2. A comparison of the model calculations and measurements reported in the literature of the chlorine dissociation fraction (—, ●) and the electronegativity (---, ×) versus argon dilution. The dotted line represents a linear fit to the measured electronegativity.

2.5. Gas pumping

In order to preserve purity, the gas in a discharge chamber is normally replenished by simultaneously pumping gas in and out of the chamber during operation. Pumping of gas into the chamber is factored into the Cl_2/Ar model by assuming the reactions



which contribute to the production of $\text{Cl}_2(v = 0)$ molecules and Ar atoms with a rate given by $R = 4.48 \times 10^{17} Q_{\{\text{Cl}_2, \text{Ar}\}}/V$, where Q_X is the flow of species X into the chamber in sccm, V is the chamber volume and the scalar converts sccm to particles/s. Argon dilution is realized by changing the ratio of Q_{Ar} to Q_{Cl_2} , and consequently the rates of Cl_2 and Ar production, while maintaining a fixed total flow rate $Q_{\text{Cl}_2} + Q_{\text{Ar}}$.

The pumping of gas out of the chamber is accounted for in a similar fashion, i.e. with the reactions



which contribute to the loss of every gas particle except the negative ion Cl^- , which is normally absent at the chamber boundaries and is therefore not pumped out. The rate coefficient for reaction (R50) is given by

$$k_{\text{po}} = 1.27 \times 10^{-5} \frac{Q_{\text{Cl}_2} + Q_{\text{Ar}}}{p_o V}, \quad (\text{18})$$

where p_o is the outlet-flow pressure in Torr and the scalar converts sccm to $\text{Torr m}^3 \text{ s}^{-1}$. The outlet-flow pressure p_o can be thought of as the pressure at the other end of the outlet-flow valve that results from increasing or decreasing its closure. In our calculations this parameter is calibrated until a particular discharge pressure p is obtained, which results in a decreasing k_{po} with an increasing discharge pressure p .

3. Results and discussion

In figure 2, the calculated chlorine dissociation fraction, $[\text{Cl}]/([\text{Cl}] + [\text{Cl}_2])$, versus argon dilution is compared with

the measurement of Fuller *et al* [13] in a stainless steel chamber of radius $R \simeq 8$ cm and length $L = 15.24$ cm at $p = 18$ mTorr, $P_{\text{rf}} = 600$ W ($P_{\text{abs}} = 450$ W) and $Q_{\text{Cl}_2} + Q_{\text{Ar}} = 35$ sccm. Although the model and the measurement agree that at high argon content the chlorine molecules are almost entirely dissociated, the measurement shows that instead of progressively increasing with argon dilution, as predicted by the model, the dissociation fraction increases rapidly as soon as the discharge is diluted with a small amount of argon. The experimental results are quite unusual, since a small addition of a noble gas is normally not expected to have such a drastic effect on the discharge properties. The model predicts a slow increase in dissociation fraction because small argon dilution has only a weak effect on the electron temperature and the electron density. This discrepancy could be explained if argon in some way drastically inhibits recombination of Cl atoms at the wall, lowering the wall recombination coefficient considerably. However, since we are unaware of any direct predictions thereof, the wall recombination coefficient has been assumed to be independent of argon dilution in this study.

Also shown in figure 2 is a comparison of the calculated electronegativity, n_-/n_e , and the measurement of Corr *et al* [11] in a stainless steel chamber with dimensions $R = 10$ cm and $L = 8.5$ cm at $p = 10$ mTorr, $P_{\text{rf}} = 200$ W ($P_{\text{abs}} = 150$ W) and $Q_{\text{Cl}_2} + Q_{\text{Ar}} = 10$ sccm. The measurement and the model are in fair agreement. Both show a decrease in electronegativity with argon content, although the measured values are larger overall. However, the measured data again shows a rapid response to a small addition of the noble gas, with electronegativity increasing almost 60% with a 10% argon dilution. The model, on the other hand, predicts no such anomalies. Instead, we find that the electronegativity n_-/n_e is directly proportional to the argon dilution, i.e. that n_-/n_e decreases by 10% when the discharge is diluted with 10% argon, for instance. The apparent peaking of the measured electronegativity at 10% argon dilution is even harder to explain than the trend in the measured dissociation fraction. It would require a number of parameters to change rapidly in favour of an increasing electronegativity, such as the dissociation fraction which would need to decrease with small argon addition, which in turn contradicts both the measurement and the model. However, a straight line least squares fit to the measured data (dotted line) is not an unreasonable one, in particular for all the points above a 10% argon dilution which fit nicely to the straight line. In fact, this straight line coincides almost perfectly with our results when multiplied by a factor of two. This indicates that the discrepancy between the model and the measurement is rather in their magnitude than in their different responses to argon dilution. A systematic difference of a factor of two can easily be regarded as satisfactory, in particular when taking into account that the electronegativity n_-/n_e includes the combined uncertainties of two measured/calculated parameters. We find that the most likely reason for the apparently underestimated electronegativity is very little production of negative ions through vibrationally excited chlorine molecules. Their density is probably underestimated in the model, which would primarily be explained by inaccurate cross-sections for

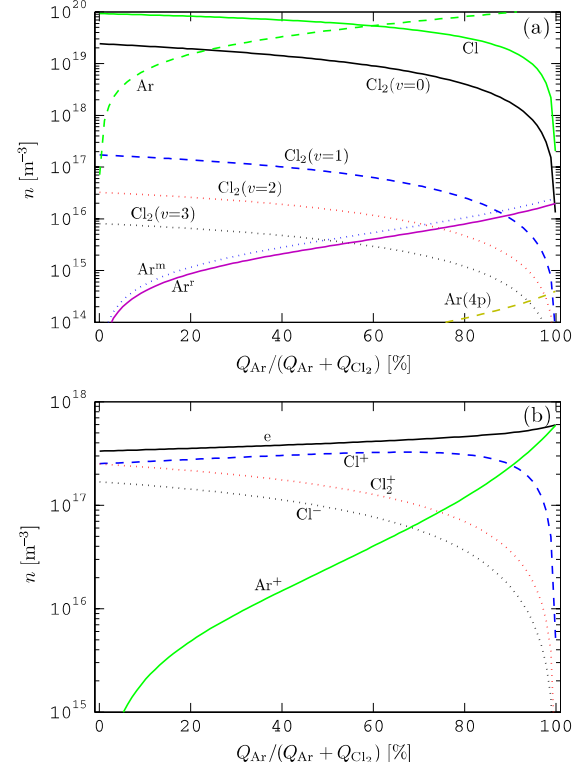


Figure 3. The densities of (a) neutral and (b) charged chlorine and argon particles versus argon dilution. The discharge pressure is $p = 10$ mTorr, the absorbed power $P_{\text{abs}} = 500$ W and the total gas flow rate $Q_{\text{Cl}_2} + Q_{\text{Ar}} = 100$ sccm. The chamber is assumed to be made of stainless steel, cylindrical with dimensions $R = 10$ cm and $L = 10$ cm.

vibrational excitation. An overestimated electron temperature and dissociation fraction are less likely reasons since comparison with measurements has shown those parameters to already rather favour increased Cl^- production in the model [1].

The neutral and charged particle densities are shown versus argon dilution in figures 3(a) and (b), respectively. The pressure is $p = 10$ mTorr, the power $P_{\text{abs}} = 500$ W and the total gas flow rate $Q_{\text{Cl}_2} + Q_{\text{Ar}} = 100$ sccm. The chamber is assumed to be made of stainless steel, cylindrical with dimensions $R = 10$ cm and $L = 10$ cm. We note that the discharge is highly dissociated with Cl atoms being the dominant neutral until the argon content is 60%. While the densities of chlorine particles generally decrease with decreasing chlorine content, the Cl^+ density increases until the argon dilution is 68%. This is likely a result of the increasing electron temperature, shown in figure 4, which increases with argon content at low and intermediate pressures but decreases at high pressures. The chlorine dissociation fraction, shown in figure 5 versus pressure for various argon concentrations, decreases with increased pressure above 10 mTorr at low and moderate argon content. As the argon content is increased the dissociation fraction also increases and becomes less dependent on pressure, decreasing much less with increasing pressure.

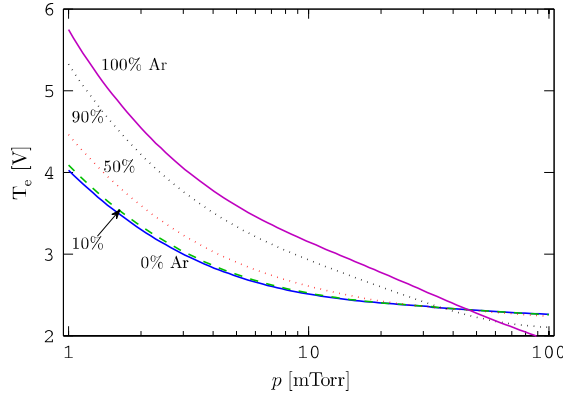


Figure 4. The electron temperature versus pressure for various argon dilutions. Conditions are as in figure 3.

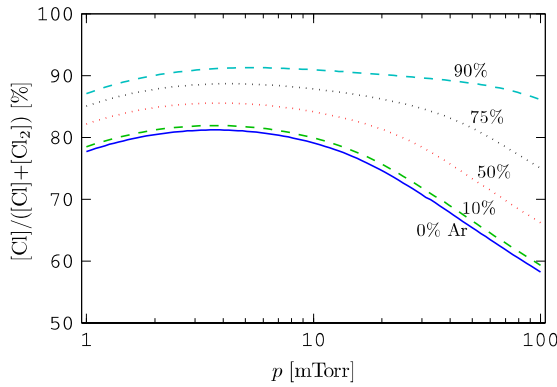


Figure 5. The chlorine dissociation fraction versus pressure for various argon dilutions. The conditions are as in figure 3.

The electronegativity n_-/n_e and the electron and negative ion densities versus argon dilution are shown in figure 6. The electronegativity, shown in figure 6(a) for various pressures, decreases with increased argon dilution, regardless of the pressure. At 10 mTorr it decreases from 0.51 for a pure chlorine discharge to 0.24 for 50% Cl₂/50% Ar. However, once the argon dilution is increased beyond $\sim 80\%$ the decrease becomes much more rapid. The decrease versus argon dilution is always proportionally similar at the other pressures. The electron density, shown in figure 6(b) for various absorbed powers, increases similarly versus argon dilution for all the powers, or between 70% and 120% from the pure chlorine to the pure argon discharge. The electron density either increases or decreases with argon content depending on the discharge pressures. While it decreases slightly with argon content at 1 mTorr, it increases by a factor of 26 at 100 mTorr. This is partly a result of the higher negative ion density at 100 mTorr which suppresses the electron density in the pure chlorine discharge but has less effect in the argon diluted discharge.

The pressure dependence of the fraction of Cl⁺ positive ions, shown in figure 7, can be modified by argon dilution. It peaks at low pressures when the argon content is low or moderate, but at high pressures in an argon dominated discharge. Furthermore, the peak value does not decrease

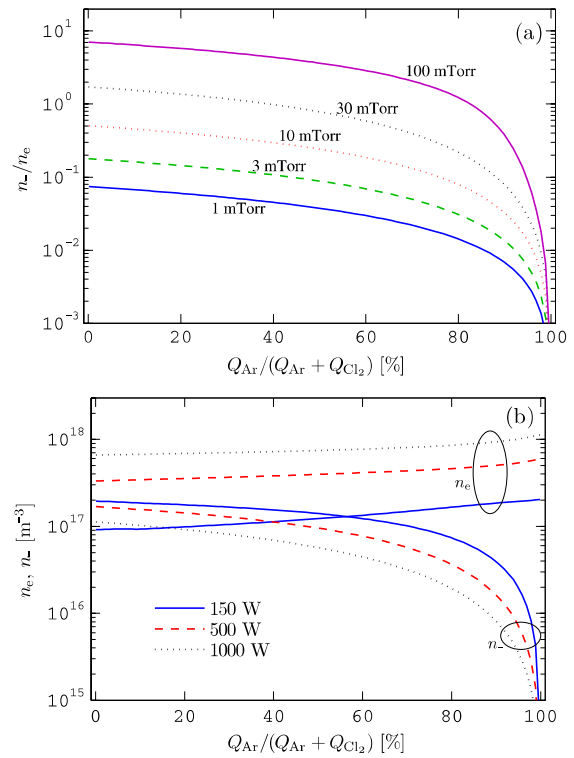


Figure 6. The influence of argon dilution on (a) the electronegativity n_-/n_e for various pressures at $P_{abs} = 500$ W and (b) the electron and negative ion densities for various absorbed powers at $p = 10$ mTorr. Other conditions are as in figure 3.

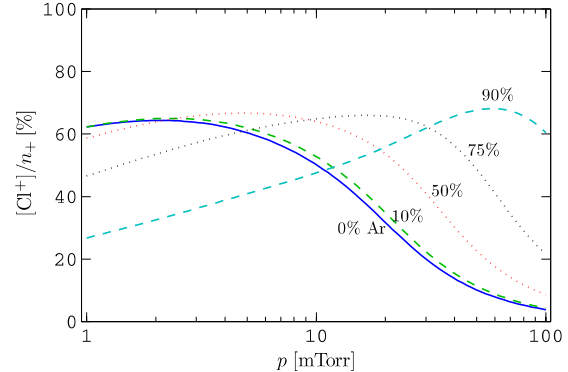


Figure 7. The fraction of Cl⁺ positive ions $n_+ = [Cl^+] + [Cl_2^+] + [Ar^+]$ versus pressure for various argon dilutions. The conditions are as in figure 3.

with increased argon content, but rather increases slightly, even when the argon content has reached 90%.

The total and relative reaction rates for the creation and destruction of Cl⁺ ions are shown in figures 8(a) and (b), respectively. Similarly to the Cl⁺ density, shown in figure 3(b), the total rate for Cl⁺ creation/destruction increases with argon content until the argon dilution is 60%. The total rates for the creation/destruction of all the other chlorine particles decrease with increasing argon content. Even in an argon dominated discharge, electron impact ionization of Cl is responsible for most of the Cl⁺ production, with charge transfer from Ar⁺,

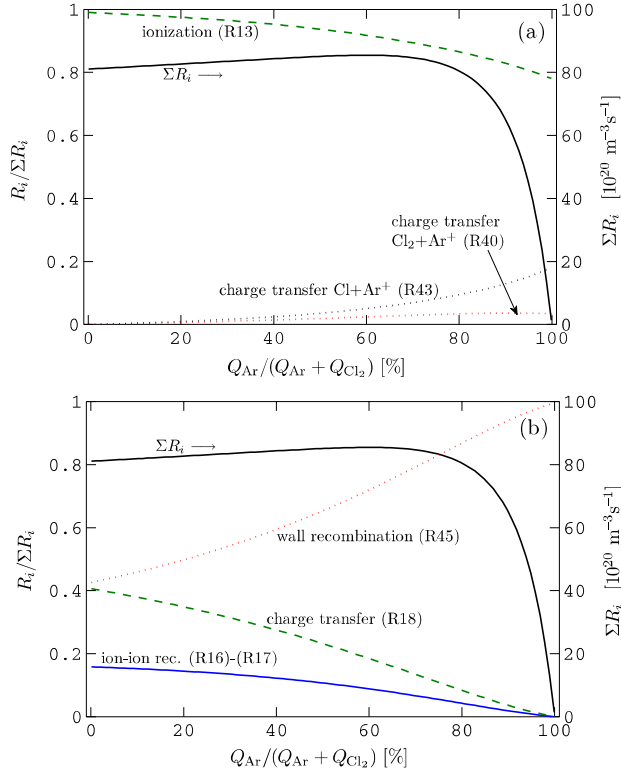


Figure 8. The total and relative reaction rates for (a) the creation and (b) the destruction of Cl^+ ions versus argon dilution. The conditions are as in figure 3.

reactions (R40) and (R43), contributing at most about 21%, combined. Being roughly 57% in a pure Cl_2 discharge, the contribution of bulk processes to the loss of Cl^+ ions decreases with increasing argon content, primarily because of the receding chlorine particle density in the discharge. Meanwhile, wall recombination of Cl^+ ions, reaction (R45), becomes the dominant pathway for Cl^+ loss at high argon content.

Electron impact ionization of Cl_2 molecules and charge transfer from Cl^+ ions are responsible for the creation of most Cl_2^+ ions, ionization becoming the dominant process at high argon content. Charge transfer from Ar^+ , reaction (R39), has only a small contribution, or at most about 9%. Argon dilution has a small effect on the loss mechanism of Cl_2^+ , with dissociative recombination (R12) and wall recombination (R45) being the most important processes as in a pure Cl_2 discharge. The same applies to the creation of the negative Cl^- ion, shown in figure 9(a), which is still entirely created by dissociative electron attachment and mostly ($\sim 95\%$) from $\text{Cl}_2(v=0)$. However, since ion-ion recombination of Cl^- with Ar^+ ions, reaction (R41), has the same rate coefficient as ion-ion recombination with Cl_2^+ and Cl^+ ions, reactions (R16) and (R17), the Cl^- loss is heavily influenced by argon dilution, as shown in figure 9(b). In an argon dominated discharge, ion-ion recombination with Ar^+ ions accounts for roughly 85% of the Cl^- loss.

The relative reaction rates for the creation and destruction of Cl atoms are shown in figures 10(a) and (b). Although

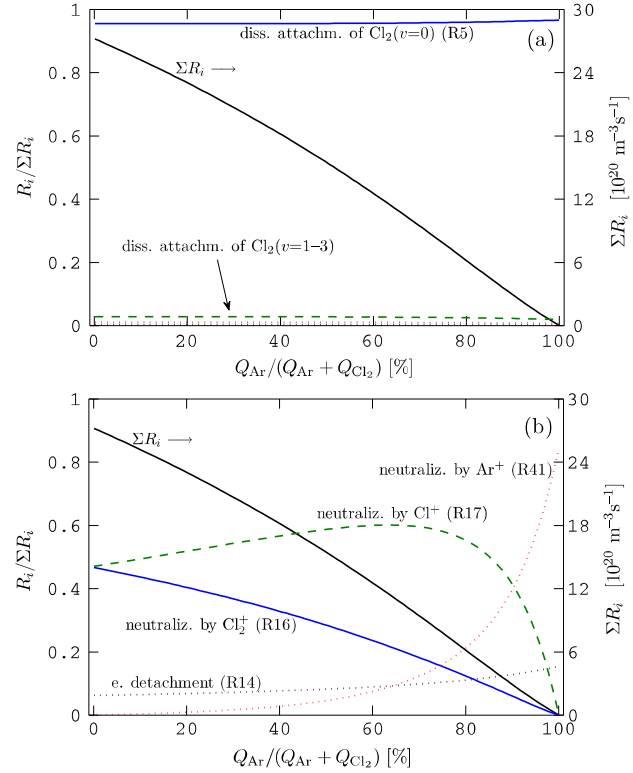


Figure 9. The total and relative reaction rates for (a) the creation and (b) the destruction of Cl^- negative ions versus argon dilution. The conditions are as in figure 3.

no argon reactions contribute significantly to the production of Cl atoms, the contribution of wall recombination of Cl^+ ions, reaction (R45), increases rapidly with increasing argon dilution, accounting for up to 56% in an argon dominated discharge. While less than 11% of Cl atoms are lost to charge transfer with Ar^+ , reaction (R43), the contribution of electron impact ionization increases from about 13% in a Cl_2 discharge to about 44% in an argon dominated discharge.

Argon–chlorine reactions, i.e. reactions (R39)–(R44) in table 1, generally have only a small effect on the creation or destruction of chlorine particles, even at high argon content. The loss of Cl^- is an exception, being mainly lost by ion–ion recombination with Ar^+ ions, reaction (R41), in an argon dominated discharge. Charge transfer from Ar^+ to Cl_2 , reaction (R39), increases the rate of Cl_2^+ production by no more than 10%. Charge transfer from Ar^+ to Cl, reaction (R43), adds at most roughly 21% to the production of Cl^+ and about 10% to the loss of Cl. Other argon–chlorine reactions have a negligible effect on the overall discharge chemistry. However, the argon dilution indirectly changes the loss/destruction mechanisms considerably because of the changing electron temperature and generally decreasing chlorine particle density. Wall recombination of ions, reaction (R45), becomes more important with argon dilution, dominating the creation of Cl atoms and loss of Cl^+ and Cl_2^+ ions for instance. Although most bulk processes become less important, the contribution of electron impact ionization generally increases with argon dilution as a result of the increased electron temperature.

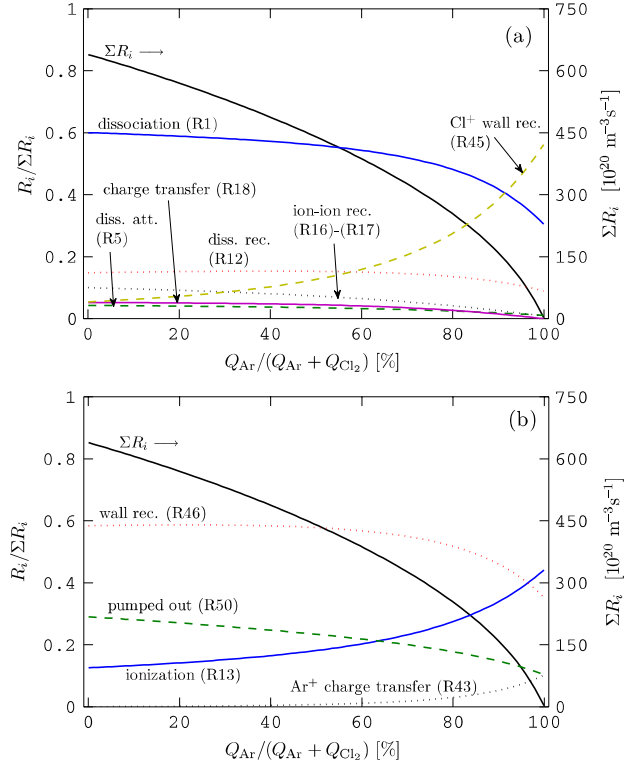


Figure 10. The total and relative reaction rates for (a) the creation and (b) the destruction of Cl atoms versus argon dilution. The conditions are as in figure 3.

While the electronegativity α has been shown to increase with pressure and decrease with power [1], the decrease with argon content is similar for every power and pressure we have explored. Because the mechanisms for both creation and loss of Cl^- ions are very simple, we can attempt to analytically determine the dependence of electronegativity on argon dilution. While Cl^- ions are entirely created by electron impact dissociative attachment, ion–ion recombination of Cl^- with positive ions is the dominating loss mechanism over a wide range of discharge conditions. Therefore,

$$k_{\text{att}} n_e [\text{Cl}_2] = k_{\text{rec}} n_+ n_- \quad (19)$$

and

$$\alpha = \frac{n_-}{n_e} = \frac{k_{\text{att}} [\text{Cl}_2]}{k_{\text{rec}} n_+}. \quad (20)$$

Now, as figure 3(b) illustrates, the positive ion density increases relatively weakly with argon dilution. Then, since the dissociative attachment rate coefficient k_{att} decreases weakly with argon dilution (because of the slowly increasing electron temperature), the ratio k_{att}/n_+ can be assumed to be almost independent of the argon fraction. If we assume that $[\text{Cl}_2] \propto \mathcal{F}_{\text{Cl}_2}$, where $\mathcal{F}_{\text{Cl}_2}$ is the fraction of Cl_2 in the gas being pumped into the chamber, we see that the electronegativity α is almost directly proportional to the fraction of chlorine gas flow, that is

$$\alpha \propto \mathcal{F}_{\text{Cl}_2} = 1 - Q_{\text{Ar}}/(Q_{\text{Ar}} + Q_{\text{Cl}_2}). \quad (21)$$

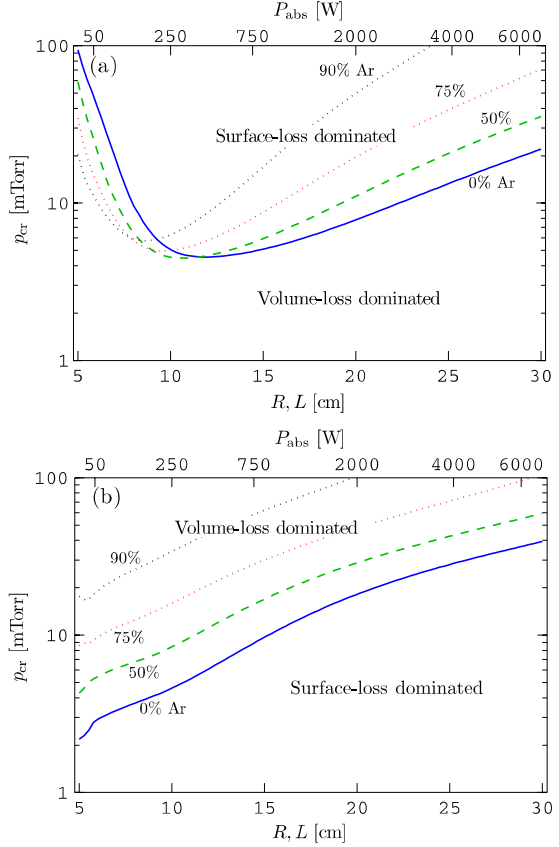


Figure 11. The critical pressure p_{cr} for (a) the dominance of surface loss over volume loss of chlorine atoms and (b) the dominance of volume loss over surface loss of positive ions (Cl^+ , Cl^- and Ar^+) versus the chamber size ($R = L$) for various argon dilutions. The power density is kept constant at $P_{\text{abs}}/V = 79.6 \text{ kW m}^{-3}$ by varying the absorbed power P_{abs} with R, L as indicated on the top axis. The total gas flow rate is $Q_{\text{Cl}_2} + Q_{\text{Ar}} = 100 \text{ sccm}$.

We found that this simple relation is in excellent agreement with the global model calculations over a wide range of conditions, i.e. for $p = 1\text{--}100 \text{ mTorr}$ and $P_{\text{abs}} = 150\text{--}1000 \text{ W}$ in a stainless steel chamber with dimensions $R, L = 10 \text{ cm}$, the electronegativity α always decreases exactly as $\mathcal{F}_{\text{Cl}_2}$. Furthermore, we have already found that a linear least squares fit to the measured electronegativity shown in figure 2 is reasonably accurate for most of the data, being in agreement with the above relation as well.

Given the high degree of dissociation in the chlorine discharge, it is believed that surface loss of Cl atoms, and subsequently the wall recombination coefficient γ_{rec} , single-handedly determines the atomic density. Figure 11(a) shows the critical pressure versus the chamber size (R, L) for surface dominated loss of neutral chlorine atoms, i.e. the pressure at which wall recombination, reaction (R46), becomes more important than pumping of Cl out of the chamber (R50), electron impact ionization (R13) and charge transfer from Ar^+ (R43), combined. The power density is kept constant by varying the absorbed power as $P_{\text{abs}} = P_{\text{abs},0} \times R^3/R_0^3$, where $P_{\text{abs},0} = 250 \text{ W}$ and $R_0 = 10 \text{ cm}$. We note that since $R = L$, the surface to volume ratio is inversely proportional

to the chamber size, i.e. $A/V \propto 1/(R, L)$. At low pressures the volume processes dominate regardless of the argon dilution or chamber size. The critical pressure reaches a minimum of 4–6 mTorr at around $R, L = 10\text{ cm}$, above which pressure the wall recombination dominates the volume losses of Cl atoms. When the chamber is this small the volume losses are dominated by pumping losses. This rapid replenishment of the discharge gas results in a small dissociation fraction which in turn directly reduces the wall recombination coefficient according to equation (17) and the surface loss rate of Cl atoms. However, since the pumping rate coefficient is inversely proportional to the volume, i.e. $k_{po} \propto 1/(R, L)^3$, the volume-loss rate decreases faster than the surface-loss rate and the critical pressure decreases rapidly with chamber size until $R, L = 8\text{--}12\text{ cm}$. For a larger chamber the critical pressure rises again when the surface-loss rate decreases due to a smaller surface to volume ratio A/V . Also the volume-loss rate increases due to the rapidly increasing contribution of ionization, which becomes the dominating volume-loss process in chambers larger than $R, L = 10\text{--}15\text{ cm}$. Since the electron temperature is slightly lower in larger chambers, the increased ionization rate is only a result of the increasing electron density as the chamber gets larger. Increasing the argon dilution increases the critical pressure in a large chamber ($R, L \gtrsim 10\text{ cm}$), making the volume loss dominate over a wider range of discharge pressures due to an increasing contribution of charge transfer from Ar^+ to Cl. Argon dilution has the inverse effect in a smaller chamber, with the surface processes becoming more important because of the decreasing contribution of pumping loss with argon dilution, as shown in figure 10(b).

Similarly to the neutral atoms, the positive ions are expected to be most efficiently lost to wall recombination. The critical pressure at which volume losses, i.e. dissociative recombination (R12), ion–ion recombination (R16), (R17) and (R41), and pumping (R50), dominate the surface losses of positive ions, reaction (R45), is shown versus the chamber dimensions R, L in figure 11(b). The rate coefficient $k_{+,wall}$ for positive ion loss at the wall, given by equation (10), depends on the surface to volume ratio and should therefore decrease as $1/(R, L)$ when R, L is increased. Nevertheless, the surface loss of positive ions dominates over a wider range of pressures when the chamber dimensions are increased. To explain this we have realized that the rates for the volume losses are suppressed more strongly due to decreasing Cl_2^+ and Cl^- densities than the surface losses are suppressed due to the decreasing $k_{+,wall}$ with increasing size. Wall recombination of positive ions only dominates below about 2 mTorr in the smallest chamber explored, while in the largest chamber it dominates at pressures up to about 40 mTorr. As the argon dilution is increased, wall recombination becomes even more important, dominating over a wider range of pressures for any given chamber size. We assign this mainly to the lower density of Cl^- , which through its participation in ion–ion recombination reactions leads to less volume loss of positive ions in the argon diluted discharge. Since the Cl^- density increases with increasing pressure [1], the pressure must be increased if volume losses are to dominate the positive ion loss,

explaining the higher critical pressure when the discharge is diluted with argon.

4. Conclusion

A global model of a continuous power Cl_2/Ar discharge has been developed and compared with measurements found in the literature, yielding reasonable agreement. The various plasma parameters have been studied as a function of argon dilution and discharge pressure, as well as the reaction mechanisms for the various chlorine particles. Although neutral Cl atoms are expected to be mostly lost to wall recombination, we found that at low pressures the volume losses dominate their loss, regardless of the chamber size. Pumping loss is the dominating volume-loss process in a small chamber, whereas in a large chamber the ionization rate is higher. Surface losses of atoms are most important in moderately sized chambers ($R, L \sim 10\text{ cm}$) where they dominate at pressures down to 4 mTorr. When the chamber gets either smaller or larger, the volume losses become increasingly more important and dominate over a wider pressure range. Diluting the discharge with argon benefits the volume losses when the chamber is large but the surface losses when it is small. Contrary to the neutral atom loss, surface losses were found to dominate the positive ion loss at low pressures. Even though the surface-loss rate coefficient decreases with increasing chamber size, the surface-loss processes dominate over a wider range as the chamber size is increased. We found that this occurs because the volume-loss processes are suppressed more strongly by the chamber size than the surface-loss processes, primarily because the Cl_2^+ and Cl^- densities decrease more rapidly with chamber size than the surface-loss rate coefficient. Dilution by argon further increases the importance of surface losses of ions, dominating over an even wider range of pressures than in the pure chlorine discharge because the negative ion density decreases when argon is added. We found that the electron temperature increases with argon dilution at low and intermediate pressures but decreases at high pressures. The chlorine dissociation fraction was found to increase and become less dependent on pressure with increased argon content, while the electronegativity decreased proportionally to the argon dilution at every power and pressure explored. The Cl^+ density was the only chlorine particle density that increased with increasing argon dilution, increasing until the argon content was almost 70%. No other extrema were found versus argon dilution. The pressure dependence of the Cl^+ fraction was found to change radically with argon content, from peaking at low pressures in a pure chlorine discharge to peaking at high pressures in an argon dominated discharge. While charge transfer from Ar^+ ions was found to increase the total rate of Cl^+ creation somewhat, most Cl^+ ions are still created by electron impact ionization of Cl atoms at high argon content. With the exception of Cl^- , whose loss can be dominated by ion–ion recombination with Ar^+ ions, argon–chlorine reactions do not have a considerable influence on the reaction mechanisms of chlorine particles. However, since the electron temperature and the chlorine particle densities are strongly affected by argon dilution, the

overall reaction mechanism is very different in a heavily argon diluted discharge than in a pure chlorine discharge at the same pressure and power.

Acknowledgments

This work was partially supported by the Icelandic Research Fund and the University of Iceland Research Fund.

References

- [1] Thorsteinsson E G and Gudmundsson J T 2010 *Plasma Sources Sci. Technol.* **19** 015001
- [2] Gu S-M, Kim D-P, Kim K-T and Kim C-I 2005 *Thin Solid Films* **475** 313
- [3] Shin M H, Na S W, Lee N-E and Ahn J H 2006 *Thin Solid Films* **506–507** 230
- [4] Hsueh K-P, Hou R-J and Tun C-J 2009 *J. Vac. Sci. Technol. B* **27** 2187
- [5] Efremov A, Min N-K, Yun S J and Kwon K-H 2008 *J. Vac. Sci. Technol. A* **26** 1480
- [6] Kim D-P, Kim K-T, Kim C-I and Efremov A M 2004 *Thin Solid Films* **447–448** 343
- [7] Efremov A, Kim D-P and Kim C-I 2004 *IEEE Trans. Plasma Sci.* **32** 1344
- [8] Efremov A, Min N-K, Choi B-G, Baek K-H and Kwon K-H 2008 *J. Electrochem. Soc.* **155** D777
- [9] Kleditzsch S and Riedel U 2000 *J. Vac. Sci. Technol. A* **18** 2130
- [10] Tinck S, Boullart W and Bogaerts A 2008 *J. Phys. D: Appl. Phys.* **41** 065207
- [11] Corr C S, Despiau-Pujo E, Chabert P, Graham W G, Marro F G and Graves D B 2008 *J. Phys. D: Appl. Phys.* **41** 185202
- [12] Fuller N C M, Herman I P and Donnelly V M 2001 *J. Appl. Phys.* **90** 3182
- [13] Fuller N C M, Donnelly V M and Herman I P 2002 *J. Vac. Sci. Technol. A* **20** 170
- [14] Bassett N L and Economou D J 1994 *J. Appl. Phys.* **75** 1931
- [15] Eddy C R, Leonhardt D, Douglass S R, Thoms B D, Shamamian V A and Butler J E 1999 *J. Vac. Sci. Technol. A* **17** 38
- [16] Thorsteinsson E G and Gudmundsson J T 2010 *J. Phys. D: Appl. Phys.* **43** 115202
- [17] Lee C, Graves D B, Lieberman M A and Hess D W 1994 *J. Electrochem. Soc.* **141** 1546
- [18] Patel K K 1998 *Master's Thesis* University of California at Berkeley, Department of Electrical Engineering and Computer Sciences
- [19] Thorsteinsson E G, Hjartarson A T and Gudmundsson J T 2008 *Technical Report RH-16-2008* Science Institute, University of Iceland
- [20] Rescigno T N 1994 *Phys. Rev. A* **50** 1382
- [21] Gudmundsson J T and Thorsteinsson E G 2007 *Plasma Sources Sci. Technol.* **16** 399
- [22] Lieberman M A and Lichtenberg A J 2005 *Principles of Plasma Discharges and Materials Processing* 2nd edn (New York: Wiley)
- [23] Christophorou L G and Olthoff J K 1999 *J. Phys. Chem. Ref. Data* **28** 131
- [24] Španěl P, Tichý M and Smith D 1993 *Int. J. Mass Spectrom. Ion Process.* **129** 155
- [25] Thorsteinsson E G and Gudmundsson J T 2009 *Plasma Sources Sci. Technol.* **18** 045001
- [26] Lee C and Lieberman M A 1995 *J. Vac. Sci. Technol. A* **13** 368
- [27] Ashida S and Lieberman M A 1997 *Japan. J. Appl. Phys.* **36** 854
- [28] Cosby P C and Helm H 1992 *Technical Report WL-TR-93-2004*, US Air Force Material Command, Wright Patterson AFB, OH 45433-7650
- [29] Basner R and Becker K 2004 *New J. Phys.* **6** 118
- [30] Calandra P, O'Connor C S S and Price S D 2000 *J. Chem. Phys.* **112** 10821
- [31] Ruf M, Barsotti S, Braun M, Hotop H and Fabrikant I 2004 *J. Phys. B: At. Mol. Opt. Phys.* **37** 41
- [32] Kurepa M V and Belić D S 1978 *J. Phys. B: At. Mol. Opt. Phys.* **11** 3719
- [33] Golovitskii A P 2000 *Tech. Phys.* **45** 532
- [34] Kolorenč P and Horáček J 2006 *Phys. Rev. A* **74** 062703
- [35] Hayes T R, Wetzel R C and Freund R S 1987 *Phys. Rev. A* **35** 578
- [36] Ali M A and Kim Y-K 2005 *Surf. Interface Anal.* **37** 969
- [37] Fritioff K, Sandström J, Hanstorp D, Ehlerding A, Larsson M, Collins G F, Pegg D J, Danared H, Källberg A and Le Padellec A 2003 *Phys. Rev. A* **68** 012712
- [38] Church M J and Smith D 1978 *J. Phys. D: Appl. Phys.* **11** 2199
- [39] Rogoff G L, Kramer J M and Piejak R B 1986 *IEEE Trans. Plasma Sci.* **14** 103
- [40] Španěl P, Tichý M and Smith D 1993 *J. Chem. Phys.* **98** 8660
- [41] Lloyd A C 1971 *Int. J. Chem. Kinet.* **3** 39
- [42] Subramonium P 2003 *PhD Thesis* University of Illinois at Urbana-Champaign
- [43] Straub H C, Renault P, Lindsay B G, Smith K A and Stebbings R F 1995 *Phys. Rev. A* **52** 1115
- [44] Ali M A and Stone P 2008 *Int. J. Mass Spectrom.* **271** 51
- [45] Mityureva A A and Smirnov V V 2004 *Opt. Spectrosc.* **97** 508
- [46] Hayashi M 2003 A set of electron–Ar cross sections with 25 excited states http://jilawww.colorado.edu/~avp/collision_data/electronneutral/hayashi.txt
- [47] Deutsch H, Becker K, Grum-Grzhimailo A N, Bartschat K, Summers H, Probst M, Matt-Leubner S and Märk T D 2004 *Int. J. Mass Spectrom.* **233** 39
- [48] Subramonium P and Kushner M J 2002 *J. Vac. Sci. Technol. A* **20** 325
- [49] Ashida S, Lee C and Lieberman M A 1995 *J. Vac. Sci. Technol. A* **13** 2498
- [50] Lieberman M A and Gottscho R A 1994 *Physics of Thin Films* vol 18 ed M Francombe and J Vossen (New York: Academic) pp 1–119
- [51] Hayashi M 2003 *Technical Report NIFS-DATA-072* National Institute for Fusion Science, Toki, Japan
- [52] Lias S G 2005 *NIST Chemistry WebBook NIST Standard Reference Database* ed P J Linstrom and W G Mallard No 69 (Gaithersburg, MD: National Institute of Standards and Technology)
- [53] Bol'shakov A, Cruden B and Sharma S 2004 *Plasma Sources Sci. Technol.* **13** 691
- [54] Donnelly V M and Malyshev M V 2000 *Appl. Phys. Lett.* **77** 2467
- [55] Tuszewski M 2006 *J. Appl. Phys.* **100** 053301
- [56] Kim S, Lieberman M A, Lichtenberg A J and Gudmundsson J T 2006 *J. Vac. Sci. Technol. A* **24** 2025
- [57] Booth J P and Sadeghi N 1991 *J. Appl. Phys.* **70** 611
- [58] Chantry P J 1987 *J. Appl. Phys.* **62** 1141
- [59] Stafford L, Khare R, Guha J, Donnelly V M, Poirier J-S and Margot J 2009 *J. Phys. D: Appl. Phys.* **42** 055206